Nanoscale

PAPER

View Article Online
View Journal | View Issue

Cite this: *Nanoscale*, 2022, **14**, 13689

A generic dual d-band model for interlayer ferromagnetic coupling in a transition-metal doped $MnBi_2Te_4$ family of materials†

Huisheng Zhang, *[a] Jingjing Zhang,[a] Yaling Zhang,[a] Wenjia Yang,[a] Yingying Wang,[a] Xiaohong Xu *[a] and Feng Liu*[b]

Received 15th June 2022,
Accepted 23rd August 2022

DOI: 10.1039/d2nr03283j

rsc.li/nanoscale

Realization of ferromagnetic (FM) interlayer coupling in magnetic topological insulators (TIs) of the $MnBi_2Te_4$ family of materials (MBTs) may pave the way for realizing the high-temperature quantum anomalous Hall effect (high-T QAHE). Here we propose a generic dual d-band (DDB) model to elucidate the energy difference ($\Delta E = E_{AFM} - E_{FM}$) between the AFM and FM coupling in transition-metal (TM)-doped MBTs, where the valence of TMs splits into d-t_{2g} and d-e_g sub-bands. Remarkably, the DDB shows that ΔE is universally determined by the relative position of the dopant (X) and Mn d-e_g/t_{2g} bands, $\Delta E_d = E^X_{e_g/t_{2g}} - E^{Mn}_{e_g/t_{2g}}$. If $\Delta E_d > 0$, then $\Delta E > 0$ and the desired FM coupling is favored. This surprisingly simple rule is confirmed by first-principles calculations of hole-type 3d and 4d TM dopants. Significantly, by applying the DDB model, we predict the high-T QAHE in the V-doped $Mn_2Bi_2Te_5$, where the Curie temperature is enhanced by doubling of the MnTe layer, while the topological order mitigated by doping can be restored by strain.

Introduction

Topological materials, such as topological insulators (TIs),[1,2] Chern insulators (CIs)[3–7] and topological semimetals,[8–10] have attracted considerable attention in recent years. In principle, a CI[3,4] can intrinsically exhibit the quantum anomalous Hall effect (QAHE) without an external magnetic field. Interestingly, the QAHE was first realized "extrinsically" in transition-metal (TM) doped three-dimensional (3D) TIs, but at a very low temperature.[5] Despite years of intensive efforts,[11–26] the observation temperature of the QAHE remains very low ranging from ~30 mK (ref. 5) to ~1 K.[27–29]

Recently, a van der Waals (vdW) $MnBi_2Te_4$ family of materials (MBTs)[30–37] have been discovered to provide an attractive material platform to explore the intrinsic QAHE. Different from the TM doped 3D TIs, MBTs are viewed as 3D TIs of Bi_2Te_3 intercalated with a magnetic MnTe layer, where the intralayer Mn atoms within a septuple layer (SL) have a long-range ferromagnetic (FM) order. However, the neighboring SLs of MBTs prefer an interlayer antiferromagnetic (AFM) coupling. Consequently, the QAHE can only be realized in odd-layered MBTs, at a low temperature (~1 K).[28] Applying an external magnetic field can significantly raise the quantization temperature up to 45 K by aligning all the MBT-layers into FM coupling.[38] It is expected that the high-temperature (high-T) QAHE can be achieved intrinsically without an external field, if the MBT can be tuned into FM interlayer coupling, and one theoretical possibility is believed to be substituting some Mn atoms with other TM elements, such as V, as proposed by density functional theory (DFT) calculations.[39–41] However, this approach remains to be confirmed by experiment. Therefore, beyond the specific case study,[39–41] a more general and deeper understanding of the effect of TM doping on the interlayer magnetic coupling in MBTs is highly desirable to guide the future experimental studies.

In this work, we propose a generic dual d-band (DDB) model to elucidate the effect of TM doping on the interlayer coupling in MBTs, by examining the energy difference ($\Delta E = E_{AFM} - E_{FM}$) between the AFM and FM coupling for different TM doped MBTs. Strikingly, the DDB shows that ΔE is universally determined by a single parameter, the relative position of the dopant (X) d-e_g/t_{2g} band and the Mn d-e_g/t_{2g} band, $\Delta E_d = E^X_{e_g/t_{2g}} - E^{Mn}_{e_g/t_{2g}}$. As long as $\Delta E_d > 0$, $\Delta E > 0$, and the FM coupling is favored. Indeed, this surprisingly simple rule is confirmed by DFT calculations of hole-type 3d and 4d TM

[a]*College of Physics and Electronic Information & Key Laboratory of Magnetic Molecules and Magnetic Information Materials of Ministry of Education & Research Institute of Materials Science, Shanxi Normal University, Taiyuan, 030031, China. E-mail: hszhang@sxnu.edu.cn, xuxh@sxnu.edu.cn*
[b]*Department of Materials Science and Engineering, University of Utah, Salt Lake City, Utah 84112, USA. E-mail: fliu@eng.utah.edu*
† Electronic supplementary information (ESI) available. See DOI: https://doi.org/10.1039/d2nr03283j

dopants, as we demonstrated below. Also, because TM doping may affect not only magnetic coupling but also the topological order of MBTs, we propose that V-doped $Mn_2Bi_2Te_5$ may exhibit the high-T QAHE under strain which restores the topological order mitigated by the doping.

Computational methods

The first-principles calculations were performed using the projector augmented wave (PAW) formalism[42] in the Vienna *ab initio* simulation package (VASP).[43] The Perdew–Burke–Ernzerhof (PBE) approximation was used to describe the exchange and correlation functional.[44] Here, we have mainly focused on the TM-doped MBTs, where one layer of Mn atoms is replaced by TMs, as shown in Fig. 1(b) and (d). To better describe the 3d electrons of TMs, the GGA+U method[45] was employed, where the on-site U and exchange interaction J parameters were set to 4.0 and 1.0 eV, respectively. A vacuum space of larger than 20 Å was used to avoid the interaction between two adjacent slabs. The plane-wave cutoff energy was set to 500 eV and all the atoms in the supercell were relaxed until the Hellmann–Feynman force on each atom was smaller than 0.01 eV $Å^{-1}$. The gamma-centered Monkhorst–Pack k-point mesh of 15 × 15 × 1 was adopted for structural optimization, and a denser k-point mesh of 30 × 30 × 1 was adopted for calculating magnetic properties. The van der Waals (vdW) correction with the Grimme (DFT-D3) method[46] was included. The Chern number, Berry curvature, and edge states were calculated to identify the topological properties using the Wannier90 and WannierTools packages.[47,48]

We have performed the Monte Carlo (MC) simulations to estimate the transition temperature T_c of all systems. Here, the Hamiltonian is $H = -J_{\text{eff}} \sum_{\langle i,j \rangle} S_i S_j$, where, J_{eff} is the effective nearest-neighbor exchange coupling, $\langle i,j \rangle$ represents the nearest neighbors, and S_i is the magnetic moment of site i. A 2 × 2 supercell is used to calculate the total energies of four competing magnetic configurations, corresponding to one FM and three AFM states.[23,26] In the calculations, we mainly consider the nearest, next-nearest, and next-next-nearest magnetic couplings, denoted as J_1, J_2, and J_3, respectively. By examining the total energies of the FM, Néel antiferromagnetic (N-AFM), stripy antiferromagnetic (S-AFM), and zigzag antiferromagnetic (Z-AFM) spin configurations, the three magnetic coupling constants can be extracted using the following three equations:

$$\begin{aligned} E_{\text{FM}} - E_{\text{N-AFM}} &= 3(J_1 + J_3)\,\vec{S}_{\text{A}} \cdot \vec{S}_{\text{B}}, \\ E_{\text{Z-AFM}} - E_{\text{S-AFM}} &= (J_1 - 3J_3)\,\vec{S}_{\text{A}} \cdot \vec{S}_{\text{B}}, \\ E_{\text{FM}} + E_{\text{N-AFM}} - E_{\text{Z-AFM}} - E_{\text{S-AFM}} &= 8J_2\,\vec{S}_{\text{A}} \cdot \vec{S}_{\text{B}}, \end{aligned} \tag{1}$$

where S_A and S_B are the spin operators on the site A and B in the honeycomb lattice, respectively. As the parameter J_1 is much larger than J_2 and J_3, these two parameters are neglected in our MC calculations.

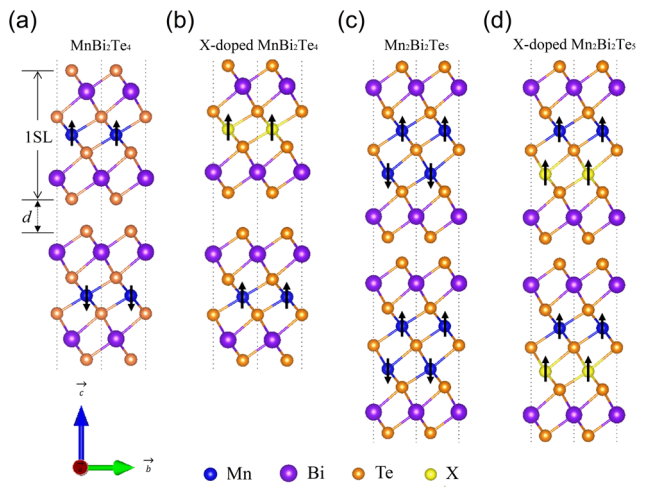

Fig. 1 Crystal structures of layered $MnBi_2Te_4$ (MBT) (a), X-doped MBT (b), $Mn_2Bi_2Te_5$ (M_2BT) (c), and X-doped M_2BT (d), where X represents transition-metal (TM) dopants. The black arrows denote the directions of the magnetic moments of TMs. Here "d" is the interlayer distance.

Results and discussion

It is known that bulk MBTs consisting of the ABC stacking Te–Bi–Te–Mn–Te–Bi–Te SL in a unit cell is an intrinsic 3D magnetic TI, in which the intralayer Mn atoms couple ferromagnetically while the two adjacent MBT SLs couple antiferromagnetically to each other, as illustrated in Fig. 1(a). The FM coupling within a SL is well understood from the Goodenough–Kanamori 90° rule, while the AFM coupling of the neighboring SLs has been explained by superexchange interaction.[49,50] This unique magnetic behavior dictates that the QAHE can only be realized in odd-layer MBTs. Moreover, the latest experiments have demonstrated that two magnetic MnTe layers can be intercalated into 3DTIs of Bi_2Te_3, forming nonuple-layer (NL) vdW crystals of $Mn_2Bi_2Te_5$ (M_2BT).[51] Similar to MBTs, M_2BTs are reported to be AFM 3DTIs, and the QAHE cannot be realized in either odd or even layers, because Mn atoms couple antiferromagnetically within and between the MnTe double layers. Therefore, realizing the FM interlayer coupling in MBTs/M_2BTs plays an important role for achieving the high-T QAHE.

Next, we propose a simple DDB model to better understand the magnetic coupling in intrinsic MBTs and the effect of doping. In layered MBTs, each Mn^{2+} ion is octahedrally bonded with six Te^{2-} ions, so that the d orbitals of Mn^{2+} ions are split into triply degenerate t_{2g} orbitals (d_{xy},d_{xz},d_{yz}) and doubly degenerate e_g orbitals ($d_{x^2-y^2}$, d_{z^2}). The exchange coupling between two interlayer Mn atoms is mediated by the p orbitals of Bi and Te. According to the super-exchange theory, because all the five d orbitals of Mn^{2+} ions are fully-filled in one layer with the same spin orientation (Hund's rule), it leads to the AFM coupling between adjacent layers with the five d orbitals of Mn^{2+} ions also fully-filled in the other layer but

with the same spin orientation to maximize the exchange interaction.

It is noted that the hopping of Mn d-electrons in MBTs is forbidden because of the large exchange splitting between spin up and down bands. To allow the hopping and enhance the FM interlayer coupling, a hole-type TM doping, *i.e.*, an X atom having less d electrons than Mn, is needed to open a channel of the same spin. Specifically, one can construct an effective mean-field DDB Hamiltonian to represent such hopping induced FM hopping, as shown in Fig. 2(a)[52] for the cases of X = Sc, Ti. Using the basis of {Mn-$t_{2g}\uparrow$, Mn-$e_g\uparrow$, X-$t_{2g}\uparrow$, X-$e_g\uparrow$, Mn-$t_{2g}\downarrow$, Mn-$e_g\downarrow$, X-$t_{2g}\downarrow$, X-$e_g\downarrow$}, the Hamiltonian of FM and AFM coupling can be respectively written as below

$$H_{\mathrm{FM}} = \begin{bmatrix} E^{\mathrm{Mn}}_{e_{g,\uparrow}} & t_1 \\ t_1 & E^{\mathrm{X}}_{t_{2g,\uparrow}} \end{bmatrix}, \tag{2}$$

$$H_{\mathrm{AFM}} = \begin{bmatrix} E^{\mathrm{Mn}}_{e_{g,\uparrow}} & t_2 & 0 & 0 \\ t_2 & E^{\mathrm{X}}_{t_{2g,\uparrow}} + U_{\mathrm{X}} & 0 & 0 \\ 0 & 0 & E^{\mathrm{Mn}}_{t_{2g,\downarrow}} + U_{\mathrm{Mn}} & t_3 \\ 0 & 0 & t_3 & E^{\mathrm{X}}_{e_{g,\downarrow}} \end{bmatrix}, \tag{3}$$

where, t_1 (t_2, t_3) is the hopping parameter between Mn-$e_{g,\uparrow}$ and X-$t_{2g,\uparrow}$ for FM coupling (Mn-$e_{g,\uparrow}$ and X-$t_{2g,\uparrow}$; Mn-$e_{g,\downarrow}$ and X-$t_{2g,\downarrow}$ for AFM coupling), U_{Mn} (U_{X}) represents the exchange splitting of Mn(x), and E is the on-site energy. As the energy scale of U_{X} and U_{Mn} are much bigger than that of other energy terms, E_{FM} and E_{AFM} can be calculated as[41]

$$E_{\mathrm{FM}} = -\frac{{t_1}^2}{\Delta E_{\mathrm{d}}}, \tag{4}$$

$$E_{\mathrm{AFM}} = -\frac{{t_2}^2}{\Delta E_{\mathrm{d}} + U_{\mathrm{X}}} - \frac{{t_3}^2}{-\Delta E_{\mathrm{d}} + U_{\mathrm{Mn}}}, \tag{5}$$

where $\Delta E_{\mathrm{d}} = E^{\mathrm{X}}_{t_{2g}} - E^{\mathrm{Mn}}_{e_g}$. For the cases of V and Cr with more than three but less than five d electrons, $\Delta E_{\mathrm{d}} = E^{\mathrm{X}}_{e_g} - E^{\mathrm{Mn}}_{e_g}$. In general, as long as $\Delta E_{\mathrm{d}} > 0$ which is satisfied by all hole-type dopants (Sc, Ti, V and Cr), $\Delta E > 0$, indicating that the FM coupling is energetically favored as confirmed by DFT calculations of doping (see Fig. 2(b)). In addition, ΔE is seen to drastically increase with decreasing ΔE_{d} as one moves from Sc to Cr, indicating that the FM interlayer coupling is easier to be realized by V and Cr doping. In contrast, for the electron-type TM dopants, *i.e.*, an X atom (Fe, Co, Ni) having more d electrons than Mn, there will be no spin channel open for Mn d-electron hopping with a low energy without spin flipping (see the ESI Fig. S1†), so that the AFM coupling will be remained. On the other hand, although our DDB model predicts a favored FM coupling for the hole-type TM doped MBTs, it also shows a very small ΔE in the range of several meV. This suggests a rather low Curie temperature (T_{c}), which makes this approach experimentally challenging.

To overcome the above difficulty, we next apply the DDB model analysis to an M_2BT monolayer. One interesting idea is that doubling the MnTe layers in M_2BTs, as shown in Fig. 1(d), may further increase the T_{c} for FM ordering, which we will confirm by using DFT calculations combined with the Monte Carlo simulations. The optimized lattice constants of TM-doped M_2BT monolayers are summarized in Table 1. As expected, the FM (AFM) interlayer coupling is found in the hole- (electron-) doped M_2BTs. We extracted ΔE_{d} from the partial density of states (PDOS) (see Fig. 3) of 3d hole-type TM-doped M_2BT monolayers, as shown in Fig. 2(b), where all have $\Delta E_{\mathrm{d}} > 0$ confirming the DDB model. Importantly, one sees that ΔE of the Cr-doped M_2BT is ~80 meV per unit cell, which is one order of magnitude larger than that of all other hole-doped MBTs, suggesting a much higher T_{c}. Here, one notices that ΔE of TM-doped MBTs is much smaller than that of TM-doped M_2BTs. This is mainly because the distance between the TM dopant and Mn in MBTs (see Fig. 1) is much larger than that in M_2BTs, so that their magnetic coupling is much weaker in MBTs. For comparison, we have extracted ΔE_{d} from the PDOS (see Fig. S2†) of 3d hole-type TM-doped MBTs, as given in Fig. 2(b), also confirming the DDB model. We have checked that this finding is not sensitive to the choice of U and vdW corrections (see Fig. S3 and S4†). Moreover, we have checked the magnetic ground states of the hole-doped M_2BT

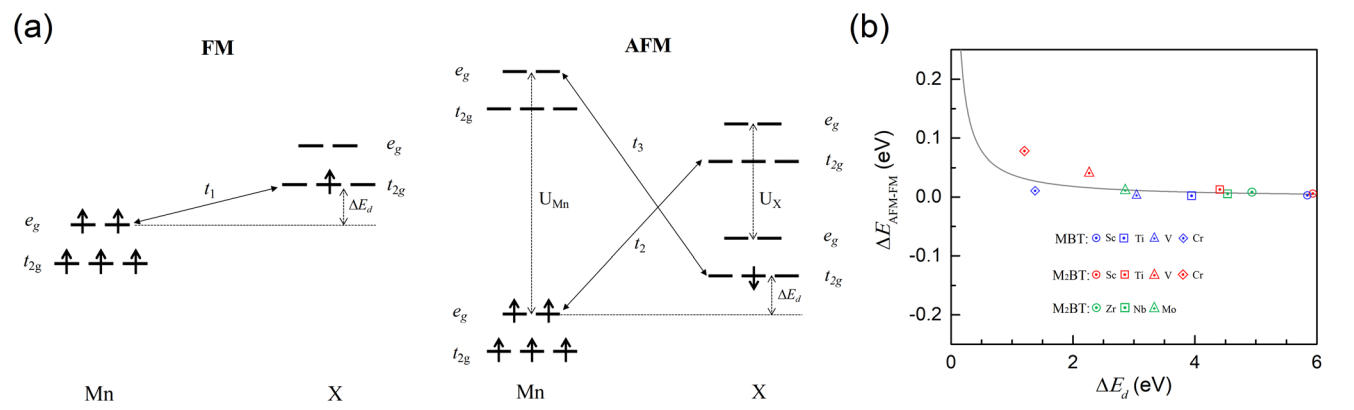

Fig. 2 (a) Schematic diagrams of FM and AFM coupling in X-doped MBTs. (b) The energy difference $\Delta E_{\mathrm{AFM-FM}}$ between AFM and FM phases as a function of ΔE_{d} (the relative position of the dopant d-t_{2g} band and the Mn d-e_g band). The parameters are set as: t_1 = 0.1 eV, t_2 = t_3 = 0.05 eV, U_{Mn} = 9.0 eV, and U_{X} = 7.0 eV. For comparison, ΔE_{d} of X-doped MBTs and M_2BTs obtained from DFT calculations is also given.

Table 1 Structural, electronic, and magnetic properties of intrinsic and X-doped $Mn_2Bi_2Te_5$ monolayers (X = Sc, Ti, V, Cr, Fe, Co, or Ni), where, a, M_X, E_G and J_1 represent the lattice constant, magnetic moments of X/Mn, bandgap, and calculated parameter of MC simulations, respectively. "M" represents that the system exhibits metallic behavior. T_c^{MC}/T_N^{MC} and T_c^{MF}/T_N^{MF} denote the estimated temperatures from the Monte Carlo simulations and mean-field theory, respectively

	Sc	Ti	V	Cr	Mn	Fe	Co	Ni
a (Å)	4.33	4.31	4.29	4.28	4.29	4.25	4.24	4.26
M_X (μ_B)	0.57	2.0	3.0	4.0	5.0	4.0	3.0	2.0
MAE (meV)	0.18	0.15	0.36	−0.46	—	—	—	—
T_c^{MC}/T_N^{MC} (K)	20	80	146	54	36	68	85	59
T_c^{MF}/T_N^{MF} (K)	26	91	169	84	33	71	109	62
E_G (eV)	M	0.07	0.29	M	0.39	M	0.14	0.11
J_1 (meV)	−0.74	−2.63	−4.87	−2.42	0.93	2.03	3.15	1.75

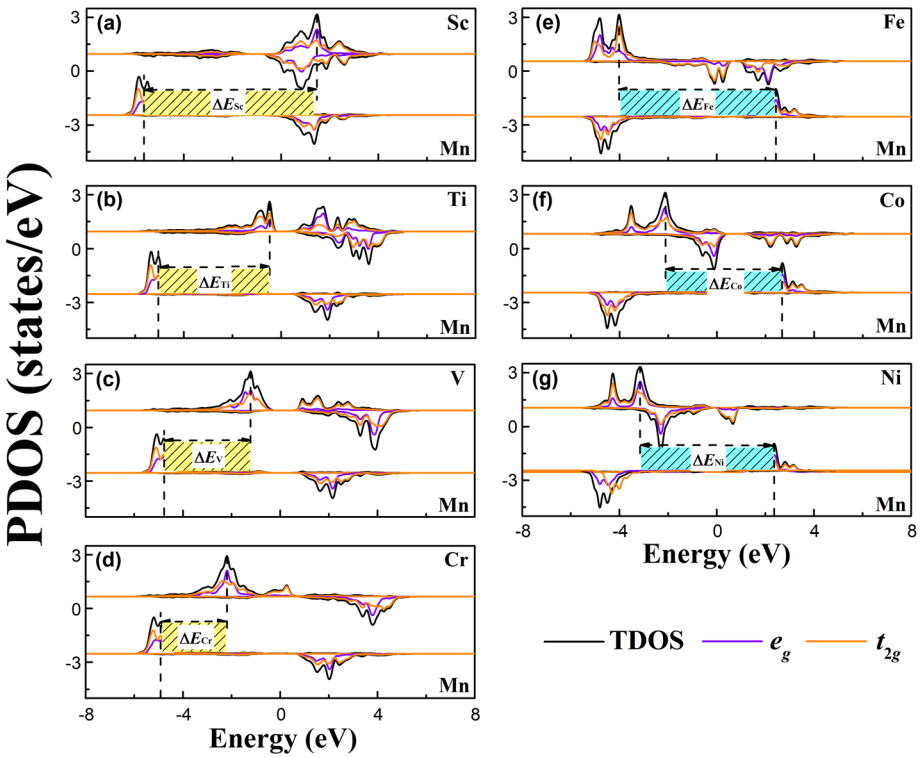

Fig. 3 Calculated partial density of states (PDOS) of Sc (a), Ti (b), V (c), Cr (d), Fe (e), Co, (f) and Ni (g)-doped M_2BT monolayers, and the PDOS of Mn is also given for each system. Fermi levels are set to zero. The vertical dashed lines mark the positions of the d-bands of TM dopants (X) and Mn, which are separated by ΔE_X. The yellow and cyan colors indicate the cases of $\Delta E_X > 0$ and $\Delta E_X < 0$, respectively.

bilayers, also showing the preferred FM over AFM coupling as displayed in Fig. S5.†

Next, we have examined the T_c or Néel temperature (T_N) of the X-doped M_2BT monolayers by performing the Monte Carlo simulations (Table 1). The T_c is ~20 K, 80 K, 146 K, and 54 K for Sc-, Ti-, V- and Cr-doped systems, respectively. Here, the estimated T_c of V-doped M_2BT is shown in Fig. 4. It is noticed that the V-doped M_2BT monolayer hosts the highest T_c rather than the Cr-doped one, which is different from the assessment based on ΔE_d. This is attributed to the fact that the V-doped system has larger J_1. We have also calculated the MAE of each system (see Table 1), where it is defined as MAE = $E_{\parallel} - E_{\perp}$, with $E_{\parallel}$ and $E_{\perp}$ denoting the total energies associated with the magnetic moment parallel and perpendicular to the plane of the 2D materials, respectively. Furthermore, we have also estimated the T_c/T_N of the X-doped M_2BTs from the mean-field theory using the formula $T_c = (2/3k_B)zS(S+1)J_1$, where, $S = 1/2$, $z = 3$ for the honeycomb lattice, and k_B is the Boltzmann constant, and the estimated T_c/T_N is listed in Table 1, and is comparable to that of the MC simulations.

Furthermore, we have double checked the electronic band structure and topology of the hole-doped M_2BT monolayers. We found that Ti- and V-doped $Mn_2Bi_2Te_5$ are insulators with a bandgap of ~70 and 290 meV, respectively, while Sc- and Cr-

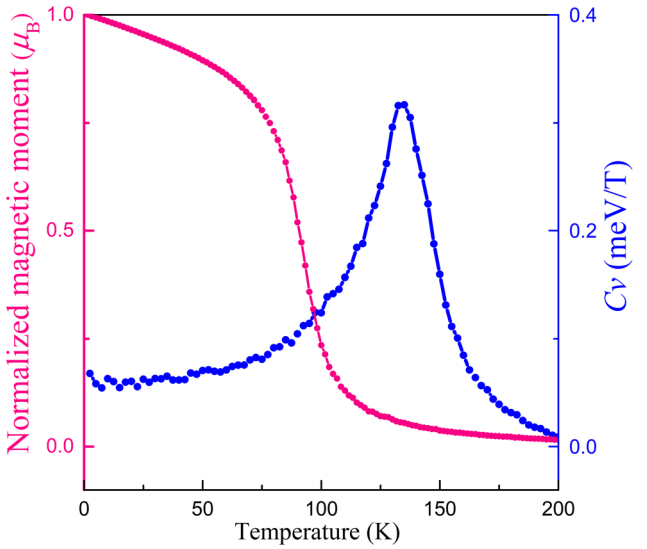

Fig. 4 Normalized magnetic moment (magenta dotted line) and specific heat C_v (blue dotted line) of the $MnVBi_2Te_5$ monolayer as a function of temperature obtained from the Monte Carlo simulations.

doped ones are metallic, as shown in Fig. S6.† Regarding the topological properties of Ti- and V-doped monolayers, the calculated Chern number $C = 0$, indicating that they are topologically trivial. Generally, the bandgap will be reduced by increasing the layer number of MBTs. Indeed, the gap of the V-doped $Mn_2Bi_2Te_5$ ($MnVBi_2Te_5$) bilayer is reduced to ~80 meV, as shown in Fig. 5(a), which remains topologically trivial with $C = 0$ (see Fig. S7†).

In order to restore the electronic topology, we propose to apply strain to induce band inversion, as shown before.[53] Thus, we have investigated the magnetic, electronic and topological properties of the $MnVBi_2Te_5$ bilayer under in-plane biaxial tensile strain.[54] The calculated results reveal that the ferromagnetism can be well preserved under strain. With increasing strain, the bandgap first closes, and then reopens (see Fig. 5(b) and (c)). The projected bands show that band inversion happens at ~4.6% tensile strain as displayed in Fig. 5(c), indicating that the strain restores the nontrivial topology. From Fig. 5(c), one also sees that the nontrivial Berry curvatures only distribute around the Γ point. The calculated $C = 1$, together with one chiral edge state appearing along the edge as shown in Fig. 5(d), demonstrates that the system is a Chern insulator exhibiting the QAHE. Moreover, our calculations reveal that the QAHE can also be realized in a strained $MnVBi_2Te_5$ trilayer, and the topological gap increases to ~16 meV under strain (see Fig. S8†). The estimated T_c of ~75 K for the strained $MnVBi_2Te_5$ trilayer suggests a high-T QAHE.

Finally, we examined the dynamic stability of the $MnVBi_2Te_5$ monolayer by calculating its phonon spectra (see Fig. S9†), which show no imaginary phonon mode. Moreover, our calculations also show that V dopants prefer periodic sublattice sites over disorder, as shown in Fig. S10,† suggesting that the growth of layered $MnVBi_2Te_5$ is experimentally feasible. We have checked three structural configurations which all give qualitatively the same results. Interestingly, from the second configuration one sees that the QAHE can also be realized in slightly disordered structures (see Fig. S11†). Furthermore, we have also checked the magnetic coupling of V-doped M_2BT with a 25% (11.1%) doping concentration, namely, only one Mn atom is replaced by one V atom in a 2 × 2 × 1 (3 × 3 × 1) M_2BT, whose crystal structures are shown in Fig. S12.† It is found that FM coupling is still preferred at all these doping concentrations, supporting the proposed DDB model.

Conclusions

In summary, we propose a generic DDB model to elucidate the energy difference ($\Delta E = E_{AFM} - E_{FM}$) between the AFM and FM coupling in the TM doped M_nBTs (n = 1, 2). Our DDB model shows that ΔE is universally determined by a single parameter, the relative position of the dopant (X) and Mn d-e_g/t_{2g} bands, $\Delta E_d = E^{X}_{e_g/t_{2g}} - E^{Mn}_{e_g/t_{2g}}$. If $\Delta E_d > 0$, then $\Delta E > 0$ and the desired FM coupling is favored. We believe that the DDB is general

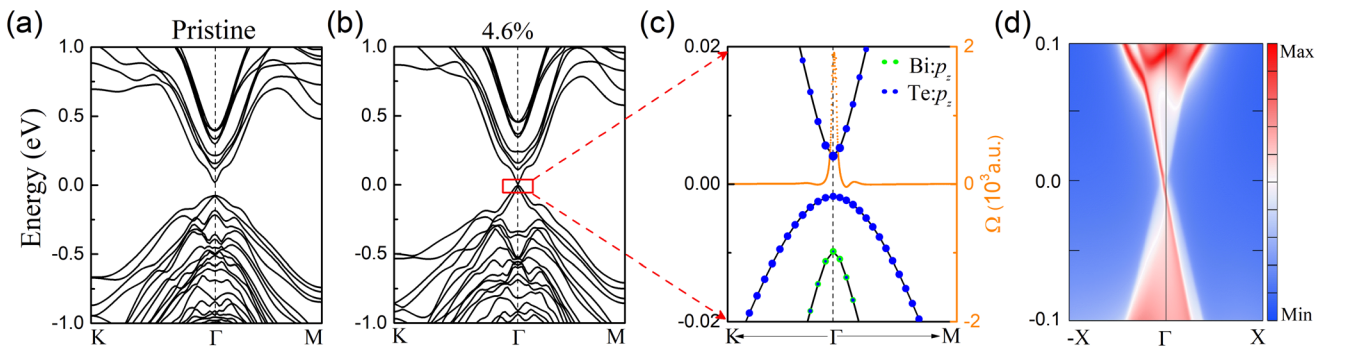

Fig. 5 Electronic band structures of pristine (a) and strained (b) V-doped M_2BT bilayers with spin–orbit coupling. (c) Magnified bands near the Fermi level in (b) showing a gap of ~5 meV, where the projected bands of the Bi-p_z and Te-p_z orbitals are also shown. The orange dotted line represents the Berry curvature distribution. (d) Edge states of the strained V-doped M_2BT bilayer, where the red and blue colors represents the contributions of the edge states. The Fermi levels are set to zero.

and applicable to other magnetic TI compounds as well, providing useful guidance for future experiments. In particular, we propose that V-doped $Mn_2Bi_2Te_5$ may exhibit the high-T QAHE under strain which restores the topological order mitigated by doping.

Author contributions

H.-S. Z. and F. L. conceived the central ideas. J. Z. carried out the calculations with substantial help from Y.-L. Z., W.-J. Y., and Y.-Y. W. H.-S. Z., X.-H. X., and F. L. wrote the manuscript. All authors discussed the results and commented on the manuscript.

Conflicts of interest

There are no conflicts to declare.

Acknowledgements

This work was supported by the National Natural Science Foundation of China (Grant Nos. 12274276, 12174237, and 51871137). F.L. acknowledges financial support from National Science Foundation Quantum Leap Big Idea under Grand No. 1936383.

References

1 M. Z. Hasan and C. L. Kane, *Rev. Mod. Phys.*, 2010, **82**, 3045.
2 X. L. Qi and S. C. Zhang, *Rev. Mod. Phys.*, 2011, **83**, 1057.
3 F. D. M. Haldane, *Phys. Rev. Lett.*, 1988, **61**, 2015.
4 R. Yu, W. Zhang, H. J. Zhang, S. C. Zhang, X. Dai and Z. Fang, *Science*, 2010, **329**, 61.
5 C. Z. Chang, J. Zhang, X. Feng, J. Shen, Z. Zhang, M. Guo, K. Li, Y. Ou, P. Wei, L. L. Wang, Z. Q. Ji, Y. Feng, S. Ji, X. Chen, J. Jia, X. Dai, Z. Fang, S. C. Zhang, K. He, Y. Wang, L. Lu, X. C. Ma and Q. K. Xue, *Science*, 2013, **340**, 167.
6 K. F. Garrity and D. Vanderbilt, *Phys. Rev. Lett.*, 2013, **110**, 116802.
7 Z. F. Wang, Z. Liu and F. Liu, *Phys. Rev. Lett.*, 2013, **110**, 196801.
8 X. Wan, A. M. Turner, A. Vishwanath and S. Y. Savrasov, *Phys. Rev. B: Condens. Matter Mater. Phys.*, 2011, **83**, 205101.
9 G. Xu, H. M. Weng, Z. Wang, X. Dai and Z. Fang, *Phys. Rev. Lett.*, 2011, **107**, 186806.
10 H. Weng, C. Fang, Z. Fang, B. A. Bernevig and X. Dai, *Phys. Rev. X*, 2015, **5**, 011029.
11 J. Hu, J. Alicea, R. Wu and M. Franz, *Phys. Rev. Lett.*, 2012, **109**, 266801.
12 H. Pan, Z. S. Li, C. C. Liu, G. Zhu, Z. Qiao and Y. Yao, *Phys. Rev. Lett.*, 2014, **112**, 106802.
13 Z. Qiao, W. Ren, H. Chen, L. Bellaiche, Z. Zhang, A. H. MacDonald and Q. Niu, *Phys. Rev. Lett.*, 2014, **112**, 116404.
14 M. Zhou, Z. Liu, W. Ming, Z. Wang and F. Liu, *Phys. Rev. Lett.*, 2014, **113**, 236802.
15 H. Zhang, T. Zhou, J. Zhang, B. Zhao, Y. Yao and Z. Yang, *Phys. Rev. B: Condens. Matter Mater. Phys.*, 2016, **94**, 235409.
16 H. Zhang, J. Zhang, T. Zhou, B. Zhao and Z. Yang, *Appl. Phys. Lett.*, 2016, **108**, 082104.
17 J. Liu, S. Y. Park, K. F. Garrity and D. Vanderbilt, *Phys. Rev. Lett.*, 2016, **117**, 257201.
18 H. Zhang, Z. Wang and X. Xu, *Appl. Phys. Lett.*, 2017, **111**, 072105.
19 Z. Liu, G. Zhao, B. Liu, Z. F. Wang, J. Yang and F. Liu, *Phys. Rev. Lett.*, 2018, **121**, 246401.
20 H. Zhang, W. Qin, M. Chen, P. Cui, Z. Zhang and X. Xu, *Phys. Rev. B: Condens. Matter Mater. Phys.*, 2019, **99**, 165410.
21 Y. Hou, J. Kim and R. Wu, *Sci. Adv.*, 2019, **5**, eaaw1874.
22 M. U. Rehman, X. Dong, T. Hou, Z. Li, S. Qi and Z. Qiao, *Phys. Rev. B: Condens. Matter Mater. Phys.*, 2019, **100**, 195422.
23 H. Zhang, W. Yang, P. Cui, X. Xu and Z. Zhang, *Phys. Rev. B: Condens. Matter Mater. Phys.*, 2020, **102**, 115413.
24 M. H. Zhang, S. F. Zhang, P. J. Wang and C. W. Zhang, *Nanoscale*, 2020, **12**, 3950.
25 S. Qi, R. Gao, M. Chang, Y. Han and Z. Qiao, *Phys. Rev. B: Condens. Matter Mater. Phys.*, 2020, **101**, 014423.
26 H. Zhang, W. Yang, Y. Ning and X. Xu, *Nanoscale*, 2020, **12**, 13964.
27 Y. Ou, C. Liu, G. Jiang, Y. Feng, D. Zhao, W. Wu, X. X. Wang, W. Li, C. Song, L. L. Wang, W. Wang, W. Wu, Y. Wang, K. He, X. C. Ma and Q. K. Xue, *Adv. Mater.*, 2018, **30**, 1703062.
28 Y. Deng, Y. Yu, M. Z. Shi, Z. Guo, Z. Xu, J. Wang, X. H. Chen and Y. Zhang, *Science*, 2020, **367**, 895.
29 M. Serlin, C. L. Tschirhart, H. Polshyn, Y. Zhang, J. Zhu, K. Watanabe, T. Taniguchi, L. Balents and A. F. Young, *Science*, 2020, **367**, 900.
30 Y. Gong, J. Guo, J. Li, K. Zhu, M. Liao, X. Liu, Q. Zhang, L. Gu, L. Tang, X. Feng, D. Zhang, W. Li, C. Song, L. Wang, P. Yu, X. Chen, Y. Wang, H. Yao, W. Duan, Y. Xu, S. C. Zhang, X. Ma, Q. K. Xue and K. He, *Chin. Phys. Lett.*, 2019, **36**, 076801.
31 M. M. Otrokov, *et al.*, *Nature*, 2019, **576**, 416.
32 M. M. Otrokov, *et al.*, *Phys. Rev. Lett.*, 2019, **122**, 107202.
33 D. Zhang, M. Shi, T. Zhu, D. Xing, H. Zhang and J. Wang, *Phys. Rev. Lett.*, 2019, **122**, 206401.
34 J. Li, Y. Li, S. Du, Z. Wang, B.-L. Gu, S.-C. Zhang, K. He, W. Duan and Y. Xu, *Sci. Adv.*, 2019, **5**, eaaw5685.
35 H. Sun, B. Xia, Z. Chen, Y. Zhang, P. Liu, Q. Yao, H. Tang, Y. Zhao, H. Xu and Q. Liu, *Phys. Rev. Lett.*, 2019, **123**, 096401.
36 L. Zhou, Z. Tan, D. Yan, Z. Fang, Y. Shi and H. Weng, *Phys. Rev. B: Condens. Matter Mater. Phys.*, 2020, **102**, 085114.
37 H. Zhang, W. Yang, Y. Wang and X. Xu, *Phys. Rev. B: Condens. Matter Mater. Phys.*, 2021, **103**, 094433.

38 J. Ge, Y. Liu, J. Li, H. Li, T. Luo, Y. Wu, Y. Xu and J. Wang, *Natl. Sci. Rev.*, 2020, **7**, 1280.
39 W. Zhu, C. Song, L. Liao, Z. Zhou, H. Bai, Y. Zhou and F. Pan, *Phys. Rev. B: Condens. Matter Mater. Phys.*, 2020, **102**, 085111.
40 Z. Li, J. Li, K. He, X. Wan, W. Duan and Y. Xu, *Phys. Rev. B: Condens. Matter Mater. Phys.*, 2020, **102**, 081107(R).
41 Y. S. Hou and R. Q. Wu, *Phys. Rev. B: Condens. Matter Mater. Phys.*, 2021, **103**, 064412.
42 G. Kresse and D. Joubert, *Phys. Rev. B: Condens. Matter Mater. Phys.*, 1999, **59**, 1758.
43 G. Kresse and J. Furthmüller, *Phys. Rev. B: Condens. Matter Mater. Phys.*, 1996, **54**, 11169.
44 J. P. Perdew, K. Burke and M. Ernzerhof, *Phys. Rev. Lett.*, 1996, **77**, 3865.
45 A. I. Liechtenstein, V. I. Anisimov and J. Zaanen, *Phys. Rev. B: Condens. Matter Mater. Phys.*, 1995, **52**, R5467.
46 S. Grimme, J. Antony, S. Ehrlich and S. Krieg, *J. Chem. Phys.*, 2010, **132**, 154104.
47 A. A. Mostofi, J. R. Yates, Y. S. Lee, I. Souza, D. Vanderbilt and N. Marzari, *Comput. Phys. Commun.*, 2008, **178**, 685.
48 Q. Wu, S. Zhang, H. F. Song, M. Troyer and A. A. Soluyanov, *Comput. Phys. Commun.*, 2018, **224**, 405.
49 J. Kanamori, *Phys. Chem. Solids*, 1959, **10**, 87.
50 H. Ehrenberg, M. Wiesmann, J. Garcia-Jaca, H. Weitzel and H. Fuess, *J. Magn. Magn. Mater.*, 1998, **182**, 152.
51 L. Cao, S. Han, Y. Y. Lv, D. Wang, Y. C. Luo, Y. Y. Zhang, S. H. Yao, J. Zhou, Y. B. Chen, H. Zhang and Y. F. Chen, *Phys. Rev. B: Condens. Matter Mater. Phys.*, 2021, **104**, 054421.
52 C. Huang, J. Feng, F. Wu, D. Ahmed, B. Huang, H. Xiang, K. Deng and E. Kan, *J. Am. Chem. Soc.*, 2018, **140**, 11519.
53 W. Liu, X. Peng, C. Tang, L. Sun, K. Zhang and J. Zhong, *Phys. Rev. B: Condens. Matter Mater. Phys.*, 2011, **84**, 245105.
54 F. Liu and M. G. Lagally, *Phys. Rev. Lett.*, 1996, **76**, 38156.